AMERICAN SOCIETY FOR MICROBIOLOGY | Applied and Environmental Microbiology®

PHYSIOLOGY

# The Acceptor Side of Photosystem II Is the Initial Target of Nitrite Stress in *Synechocystis* sp. Strain PCC 6803

**Xin Zhang,[a,b] Fei Ma,[a,b] Xi Zhu,[a,b] Junying Zhu,[c] Junfeng Rong,[c] Jiao Zhan,[a] Hui Chen,[a] Chenliu He,[a] Qiang Wang[a]**

Key Laboratory of Algal Biology, Institute of Hydrobiology, Chinese Academy of Sciences, Wuhan, Hubei, China[a]; University of Chinese Academy of Sciences, Beijing, China[b]; SINOPEC Research Institute of Petroleum Processing, Beijing, China[c]

**ABSTRACT** Nitrite, a common form of inorganic nitrogen (N), can be used as a nitrogen source through N assimilation. However, high levels of nitrite depress photosynthesis in various organisms. In this study, we investigated which components of the photosynthetic electron transfer chain are targeted by nitrite stress in *Synechocystis* sp. strain PCC 6803 cells. Measurements of whole-chain and photosystem II (PSII)-mediated electron transport activities revealed that high levels of nitrite primarily impair electron flow in PSII. Changes in PSII activity in response to nitrite stress occurred in two distinct phases. During the first phase, which occurred in the first 3 h of nitrite treatment, electron transfer from the primary quinone acceptor ($Q_A$) to the secondary quinone acceptor ($Q_B$) was retarded, as indicated by chlorophyll (Chl) *a* fluorescence induction, S-state distribution, and $Q_A^-$ reoxidation tests. In the second phase, which occurred after 6 h of nitrite exposure, the reaction center was inactivated and the donor side of photosystem II was inhibited, as revealed by changes in Chl fluorescence parameters and thermoluminescence and by immunoblot analysis. Our data suggest that nitrite stress is highly damaging to PSII and disrupts PSII activity by a stepwise mechanism in which the acceptor side is the initial target.

**IMPORTANCE** In our previous studies, an alga-based technology was proposed to fix the large amounts of nitrite that are released from $NO_X$-rich flue gases and proved to be a promising industrial strategy for flue gas $NO_X$ bioremediation (W. Chen et al., Environ Sci Technol 50:1620–1627, 2016, https://doi.org/10.1021/acs.est.5b04696; X. Zhang et al., Environ Sci Technol 48:10497–10504, 2014, https://doi.org/10.1021/es5013824). However, the toxic effects of high concentrations of nitrite on algal cells remain obscure. The analysis of growth rates, photochemistry, and protein profiles in our study provides important evidence that the inhibition by nitrite occurs in two phases: in the first phase, electron transfer between $Q_A^-$ and $Q_B$ is retarded, whereas in the second, the donor side of PSII is affected. This is an excellent example of investigating the "early" inhibitory effects (i.e., within the first 6 h) on the PSII electron transfer chain *in vivo*. This paper provides novel insights into the mechanisms of nitrite inhibition of photosynthesis in an oxygenic phototrophic cyanobacterium.

**KEYWORDS** PSII, *Synechocystis* sp. strain PCC 6803, nitrite stress

**Received** 25 October 2016 **Accepted** 13 November 2016

**Accepted manuscript posted online** 18 November 2016

**Citation** Zhang X, Ma F, Zhu X, Zhu J, Rong J, Zhan J, Chen H, He C, Wang Q. 2017. The acceptor side of photosystem II is the initial target of nitrite stress in *Synechocystis* sp. strain PCC 6803. Appl Environ Microbiol 83:e02952-16. https://doi.org/10.1128/AEM.02952-16.

**Editor** Haruyuki Atomi, Kyoto University



Address correspondence to Qiang Wang, wangqiang@ihb.ac.cn.

Over the past century, increased consumption of fossil fuels, a growing demand for nitrogen in agriculture and industry, and pervasive inefficiencies in nitrogen use have sharply increased anthropogenic nitrogen fluxes in the environment and consequently altered the global nitrogen cycle (1, 2). Nitrite, as an intermediate of the nitrogen cycle, is involved in at least three distinct biochemical pathways, namely,

nitrification, denitrification, and dissimilatory or assimilatory nitrate reduction to ammonium (3). Although nitrite is widespread, its concentration is in the micromolar range in a healthy natural environment (4). However, there have been reports of high nitrite concentrations occurring in both terrestrial and aquatic ecosystems (5–7). Imbalances in nitrification and denitrification, resulting from the inhibition or disruption of steps in these processes, can cause nitrite accumulation in aquatic systems (3, 8). Anthropogenic inputs of nitrite to the ecosystem arise from agricultural effluents, industrial discharges, and the release of wastes and sewage (9, 10). Furthermore, large amounts of nitrite have been proven to be transformed from $NO_x$-rich flue gases, which are discharged during combustion of fossil fuels (11, 12). In our previous study, we developed a method to fix the salts in flue gas from the caprolactam production plant of Sinopec's Shijiazhuang Refining & Chemical Company in China. Use of the flue gas fixed salts (i.e., $NO_2^-$ and $NO_3^-$, at a ratio of 19:1) for cultivation of microalgae has been suggested to be a promising industrial strategy for flue gas biotreatment.

Nitrite, a common form of combined inorganic nitrogen, can be assimilated as the nitrogen source for many species of plants and algae (13, 15). External nitrite is transported into cells by an active nitrate/nitrite transporter (NRT) and then reduced to ammonium by nitrite reductase (NiR), which is conserved from cyanobacteria to higher plants (16–18). The resulting ammonium is incorporated into carbon skeletons via the glutamine synthetase and glutamate synthase cycle. Although plants and cyanobacteria have essentially the same metabolic pathways for nitrite assimilation, the types of transporters in these organisms differ. Two types of NRT exist in cyanobacteria: the ABC-type NRTs, comprised of the NrtA, NrtB, NrtC, and NrtD proteins; and the major facilitator superfamily (MFS) family transporter, encoded by the *nrtP* gene (19, 20). The cyanobacterial nitrite assimilation pathway has far fewer transporters, enzymes, and regulators than does the nitrite assimilation pathway in eukaryotic cells and appears to be much simpler. In organisms that perform oxygenic photosynthesis, nitrite reduction is functionally linked to photosynthesis. Reduced ferredoxin (Fd), produced directly by the photosynthetic electron transport (ET) system, has been shown *in vivo* to be the electron donor for nitrite reductase in chloroplasts and cyanobacterial cells (21).

The optimal nitrite concentration for growth varies for different species of algae and higher plants (22, 23). In the presence of excess nitrite, organisms can accumulate toxic levels of $NO_2^-$ (24–26). Previous research showed that isolated chloroplasts subjected to high concentrations of nitrite exhibited decreased chlorophyll (Chl) contents, restricted photosynthetic electron transfer rates (27), and redistribution of absorbed excitation energy between the two photosystems (PS) (28). Photosystem II (PSII) has long been considered the target of excess nitrite in isolated thylakoid membranes (29, 30). Thermoluminescence studies (31) and loss of $S_2$ state multiline electron paramagnetic resonance (EPR) signal (26, 32) in nitrite-treated samples suggest that nitrite acts on the donor side of PSII, most likely at the manganese (Mn) cluster of the oxygen-evolving complex (OEC).

Although experimental observations indicate that high levels of nitrite induce donor-side damage in PSII *in vitro*, this hypothesis remains to be tested *in vivo*. In addition, most studies evaluating the effect of nitrite stress on PSII in isolated systems were carried out in the steady-state adapted stage. Little is known about how the initial stages of nitrite stress affect the two photosystems. These early responses may be crucial for determining the location of the primary site of damage induced by elevated nitrite concentrations. In this work, we investigated the effect of nitrite stress on photosynthesis in the cyanobacterium *Synechocystis* sp. strain PCC 6803 (here, *Synechocystis*), a model system for photosynthetic studies. We conducted a time course analysis of the structural and functional rearrangements of the photosynthetic apparatus that occur during acclimation of cyanobacteria to high levels of nitrite.

## RESULTS

**Growth characteristics of *Synechocystis* at different nitrite concentrations.** To evaluate the dose effects of nitrite on *Synechocystis* growth, we measured the growth

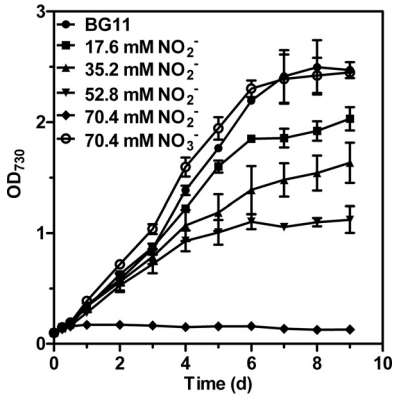


**FIG 1** Growth curves of *Synechocystis* treated with various concentrations of $NaNO_2$. The control, BG11 medium (solid circle), contained 17.6 mM $NaNO_3$ as the sole nitrogen source. Each value represents the mean ± SD of the results of at least five independent measurements.

rates of algal cultures exposed to $NaNO_2$ concentrations ranging from 17.6 to 70.4 mM (Fig. 1). The increase in cell density was followed for 9 days until the stationary-growth phase was reached for most treatments. After 12 h of exposure to nitrite, the growth rates of the control cells and cells treated with nitrite differed. An analysis of cells grown in the presence of 17.6 mM (1×), 35.2 mM (2×), or 52.8 mM (3×) $NO_2^-$ in modified BG11 media showed that the growth rate decreased with increasing concentrations of $NO_2^-$. For nitrite concentrations of above 70.4 mM (4×) $NO_2^-$, cell propagation was completely inhibited. Interestingly, despite the complete inhibition of cell growth at 4× $NO_2^-$, we did not observe any decrease in cell density during the 3-day cultivation period in 4× $NO_2^-$. Furthermore, the cells retained their viability after 12 h of treatment with 4× $NO_2^-$ if the cells were subsequently washed with N- medium and transferred to agar plates containing BG11 medium (see Fig. S1 in the supplemental material). In comparison, cell growth in the presence of 4× $NO_3^-$ showed growth rates similar to those of the BG11 control, implying that growth inhibition mediated by 4× $NO_2^-$ is attributable to the added nitrite and not to general ion effects. Thus, 4× $NO_2^-$ was used to induce nitrite stress in our subsequent analysis, as this concentration had a strong effect on cyanobacterial growth.

**The sensitivity of PSII to nitrite stress.** To investigate the effects of nitrite stress on photosynthetic activity, *Synechocystis* cells in the mid-logarithmic-growth phase were harvested, washed, and transferred to modified BG11 medium containing 4× $NO_2^-$. The time course changes of light-saturated whole-chain and PSII-mediated electron transport activities in intact cells were measured in response to nitrite stress and are shown as percentages of the corresponding control values (Fig. 2), and their absolute value changes were also plotted and are given in Fig. S2. As shown in Fig. 2, the addition of 4× $NO_2^-$ immediately inhibited photosynthetic activity. After 30 min of exposure to nitrite shock, the rate of PSII electron transport from water to phenyl-p-benzoquinone (BQ), which accepts electrons from $Q_B$, had decreased sharply to about 36% of the original activity and remained unchanged in the period of time that followed. In contrast, the whole-chain activity ($H_2O$-$CO_2$) dropped to 90% of the original activity in the first 1.5 h of nitrite treatments and subsequently slightly decreased with time. Because the percentage of decrease in PSII activity appeared to be greater than that in whole-chain activity, we postulate that PSII has substantially higher sensitivity to nitrite stress than does PSI.

To gain insight into the functional status of PSII during acclimation to nitrite stress, we determined the PSII photochemical efficiency, i.e., the ratio of variable chlorophyll fluorescence to maximum chlorophyll fluorescence ($F_v/F_m$), in the presence or absence of 3-(3,4-dichlorophenyl)-1,1-dimethylurea (DCMU). Time course analysis showed that $F_v/F_m$ decreased slightly during the first 3 h of excess-nitrite treatment (Fig. 3A). In addition, PSII-mediated electron transport activity was more sensitive to nitrite stress

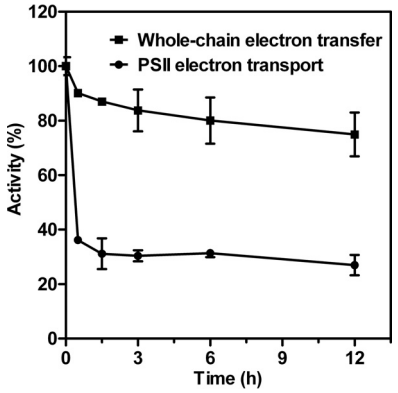


**FIG 2** Time course changes of light-saturated whole-chain and PSII-mediated electron transport activities in intact cells in response to 70.4 mM (4×) $NO_2^-$. The data are given as percentages of the corresponding control values. The activities corresponding to 100% for the untreated cells are about 137 and 234 $\mu$mol $O_2$ (mg Chl)$^{-1}$ h$^{-1}$ for whole-chain and PSII electron transport processes, respectively. Data are means ± SD ($n$ = 5).

than was the $F_v/F_m$ parameter, suggesting that the changes in the PSII induced by nitrite stress most likely occur at the oxidizing or reducing side of PSII rather than at the reaction center during the first 3 h. A second significant decrease in $F_v/F_m$ (one-way analysis of variance [ANOVA] test between cells with high nitrite treatment and control,

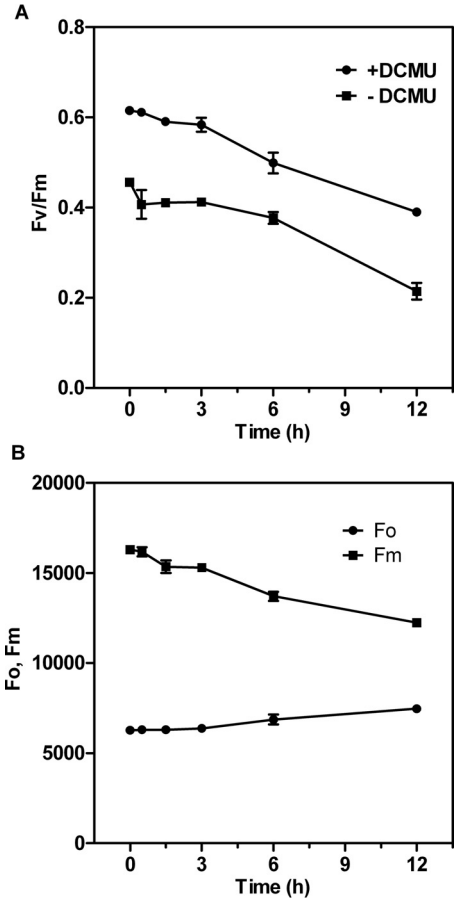


**FIG 3** Time course changes of Chl fluorescence parameters in *Synechocystis* cells incubated with 70.4 mM (4×) $NO_2^-$. (A) Maximum quantum yields of PSII ($F_v/F_m$) with or without 20 $\mu$M DCMU. (B) Minimal fluorescence level ($F_o$) in the dark-adapted state and maximal fluorescence level ($F_m$) in the presence of 20 $\mu$M DCMU at the closed PSII center. Values are given as means or means ± SD ($n$ = 5).

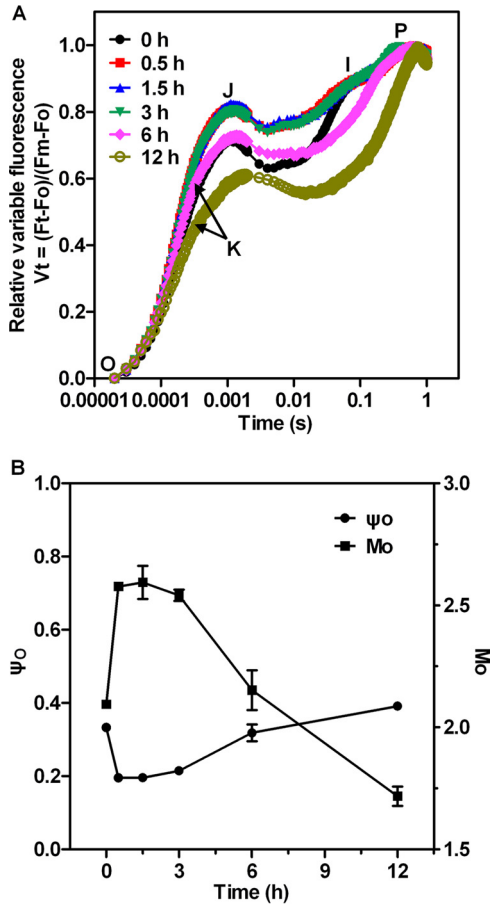


**FIG 4** The relative variable fluorescence parameters (A) and JIP-test parameters (B) in *Synechocystis* cells at different periods after the addition of 70.4 mM (4×) $NO_2^-$. $M_o$, the initial slope of the relative variable fluorescence curve; $\psi_o$, the efficiency of electron transfer from $Q_A^-$ to $Q_B$. Values represent means or means ± SD ($n = 5$).

$P < 0.05$) occurred between the 6- and 12-h time points, declining to 63% of the initial value observed in untreated cells by 12 h. The sharp decrease in $F_v/F_m$ after 6 h of high nitrite treatment was due to a considerable increase in the minimal fluorescence level ($F_o$) (one-way ANOVA test between cells with excess-nitrite treatment and control, $P < 0.01$) and a significant decrease in $F_m$ (one-way ANOVA test between cells with excess-nitrite treatment and control, $P < 0.05$) (Fig. 3B). The pronounced increase in $F_o$ during this period can be attributed to inactivation of the PSII photochemical reaction and to detachment of phosphate-buffered saline (PBS) from the PSII reaction center complexes (33).

**Polyphasic Chl *a* fluorescence induction kinetics.** To localize the action site of nitrite stress in the PSII electron transport chain, we monitored the polyphasic rise of Chl *a* fluorescence induction (FI) kinetics in *Synechocystis* cells exposed for 12 h to 4× $NO_2^-$. Before the high-nitrite treatment, *Synechocystis* cells exhibited a typical FI kinetic, called the O-J-I-P fluorescence transient, similar to that described previously (34–36) (see Fig. 4). The J, I, and P steps occurred at about 2 ms, 30 ms, and 400 ms, respectively. The O-J-I-P transient represents the successive reduction of the electron acceptor pools of PSII. The J step reflects the peak concentrations of $Q_A^-Q_B$ and $Q_A^-Q_B^-$ (with $Q_A$ and $Q_B$ being the first and second quinone electron acceptors of PSII, respectively), as demonstrated by experimental results and theoretical simulations (37). It has also been suggested that the intermediate I step reflects accumulation of $Q_A^-Q_B^{2-}$, whereas the P step indicates accumulation of $Q_A^-Q_B^{2-}$ and $PQH_2$ (34).

Figure S3 shows the original FI curves of the samples measured at different periods of exposure to excess levels of nitrite. The fluorescence intensity of the O-J-I-P curve was slightly reduced during the first 3 h of high-nitrite treatment. Compared to the initial FI curve, significant differences were observed between 6 and 12 h after treatment. During this period, the curve corresponding to the J-I-P phase leveled off. The O-J-I-P curve showed an increase at the O step and a large depression at the P step, in line with the results of the Chl fluorescence experiment (Fig. 3). The higher fluorescence emission at O and corresponding decrease in maximum fluorescence $F_P$ (Fig. S3) might be attributable to an increase in the concentration of $Q_B$-non-reducing PSII centers.

In Fig. 4A, the FI traces are normalized between $F_o$ and $F_m$ and plotted as $V_t$ changes on a logarithmic scale [$V_t = (F_t - F_o)/(F_m - F_o)$]. From these curves, it is clear that the relative variable intensity at the J step ($V_J$) was enhanced in the first 3 h of high-nitrite treatment. A similar increase at the J step was also observed in previous studies examining the effect of NaCl stress on cyanobacterial *Spirulina platensis* cells (38). This increase in $V_J$ was due to a reduction in the rate of $Q_B$-mediated $Q_A^-$ reoxidation. However, the intermediate J–I phase is clearly diminished during 6 to 12 h after nitrite stress. It has been reported that a deactivated reaction center and the absence of a transmembrane proton gradient in PSII could be related to the lack of the intermediate I level (35). In addition, an early step around 300 $\mu$s after exposure to high-intensity actinic light, which has been labeled K, emerged at 6 h of nitrite stress and became more apparent thereafter. The appearance of the K step is used as a convenient stress indicator and is specifically attributed to damage of the OEC on the electron donor side (39). Our results indicate that the structure of the thylakoid membrane was severely damaged both on the donor side and at the reaction center of PSII between 6 and 12 h after high-nitrite treatment. Further, $V_J$ was reduced and the J step occurred more than 2 ms after exposure to actinic light in cells that had been subjected to a 12-h treatment with $4\times NO_2^-$, due to the loss of the I step and the occurrence of the K step in the presence of high levels of nitrite.

To investigate the effect of nitrite stress on electron transport at the acceptor side of PSII, we obtained quantitative information from the JIP-test parameters (see Materials and Methods). During the first 3 h of exposure to high-nitrite levels, $M_0$ (the initial slope of the relative variable fluorescence curve) increased by about 23% and $\psi_0$ (i.e., the probability that a trapped exciton moves an electron into the electron transport chain beyond $Q_A$) decreased by 40% (Fig. 4B). We can therefore deduce that electron transfer on the acceptor side of PSII between $Q_A$ and $Q_B$ is inhibited by nitrite stress during the first 3 h of excess-nitrite treatment. In addition, the absence of the I phase during 6 to 12 h after nitrite stress, which was caused by inactivation of PSII reaction center, reduced $M_0$ and increased $\psi_0$ over time. Also, the changes of JIP parameters cannot characterize the damage of the acceptor side in this period.

The results described above indicate that the response of PSII photochemistry to high nitrite levels in *Synechocystis* cells consists of two distinct phases. The first phase occurs within 3 h of exposure to excess nitrite. The changes in JIP-test parameters and the negligible reduction in Chl fluorescence parameters indicate that electron transfer between $Q_A^-$ and $Q_B$ is greatly retarded. The second phase occurs after 6 h of excess-nitrite treatment. A significant decrease in $F_v/F_m$, the loss of the intermediate I level, and the occurrence of the K step suggest that nitrite stress during this phase damages the donor side of PSII, as well as the reaction center.

**Effects of nitrite stress on thermoluminescence (TL) characteristics.** Thermoluminescence (TL) is a useful technique for monitoring the functioning of the OEC and of the quinone electron acceptors. When preilluminated samples are cooled and then heated in darkness, the positive charges stored in the $S_2$ and $S_3$ oxidation states of the water-oxidizing complex recombine with electrons stabilized on the reduced $Q_A$ and $Q_B$ acceptors of PSII, leading to characteristic TL emissions (40). The TL intensity is proportional to the amount of recombining charges, whereas the peak temperature

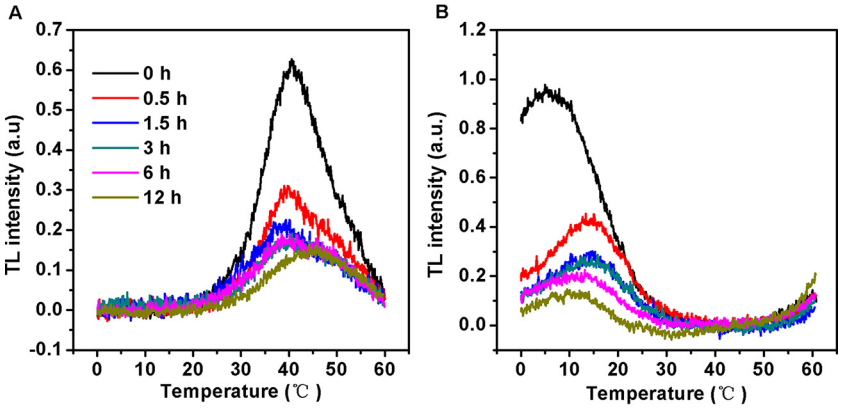


**FIG 5** Thermoluminescence glow curves of *Synechocystis* cells exposed to 70.4 mM (4×) $NO_2^-$ for up to 12 h. The cells were excited with a single-turnover saturating flash at 0°C in the absence (A) and presence (B) of 20 $\mu$M DCMU for the B and Q bands, respectively. Values represent means of the results of five independent measurements.

reflects the energetic stabilization of the separated charge pair; the higher the peak temperature, the greater the stabilization.

Excitation of *Synechocystis* cells with a single saturating light flash at 0°C prior to freezing yielded a typical B-band, which appears at around 40°C and arises largely from $S_2Q_B^-$ recombination. The amplitude of the B band was rapidly reduced within 1.5 h of excess-nitrite treatment (Fig. 5A). The TL intensity of the B band continued to decline over time. In all cases (41), a loss in the intensity of the $S_2Q_B^-$ peak is considered to be indicative of the inhibition of electron transfer from reduced $Q_A$ to $Q_B$. In addition, the B band did not shift in the first phase, whereas it was partly and fully upshifted to 45°C at 6 h and 12 h, respectively (Fig. 5A), confirming the increased energetic stability of the $S_2Q_B^-$ charge pair.

If electron transfer between $Q_A$ and $Q_B$ is blocked by DCMU, the Q band, originating from $S_2Q_A^-$ charge recombination at around 5°C, appears in place of the B band. As shown in Fig. 5B, the Q band intensity rapidly declined within 12 h of exposure to high-nitrite levels. Moreover, nitrite stress resulted in an upshift of the peak temperatures for $S_2Q_A^-$ charge recombination, relative to results seen with untreated cells. Since the increased stabilizations of the $S_2Q_B^-$ and $S_2Q_A^-$ charge recombination occurred approximately in parallel during the second phase, it seems most likely that these changes were due largely to a modification of the OEC specifically affecting the properties of the $S_2$ state.

Figure 6 shows the flash-induced oscillation of the B band intensity in nitrite-stressed *Synechocystis* cells, which reflects the redox cycling of the S states. In control cells not subjected to nitrite treatment, the B band oscillated with a periodicity of 4, with the maximum emission occurring after the second flash. This is the same type of oscillation as that observed in the cyanobacteria (42, 43). In the 6-h period following the addition of excess nitrite, the cells showed a oscillation pattern similar to that seen in the control. However, the period-4 oscillation pattern was barely observable at 12 h, indicating that advancement of the S-state cycle of the OEC was blocked beyond $S_2$ and that the OEC was impaired. Considering that the reaction center was deactivated after 6 h of excess-nitrite treatment, as revealed by the Chl fluorescence parameters (Fig. 3) and O-J-I-P transient (Fig. S3), we conclude that the donor side of PSII is less sensitive to nitrite stress than is the reaction center during the second phase.

**Effects of nitrite stress on $Q_A^-$ reoxidation kinetics.** The O-J-I-P traces and TL glow curves described above indicate that the reoxidation of $Q_A^-$ was likely retarded in response to high nitrite levels. This possibility was verified by measuring the $Q_A^-$ reoxidation kinetics in cells exposed to nitrite for different periods of time (Fig. 7). Quantitative evaluation of these decay curves was performed by fitting these curves to

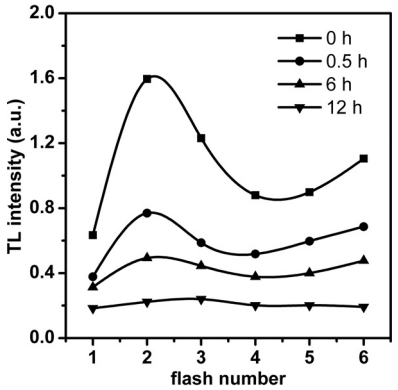


**FIG 6** Flash-induced oscillation of the B thermoluminescence band in *Synechocystis* cells at different intervals after the addition of 70.4 mM (4×) $NO_2^-$. The samples were excited by 1 to 6 single saturating flashes at 0°C, and the intensity of the thermoluminescence B band was measured. The B band intensity (indicated in a.u. [arbitrary units]) is plotted as a function of the number of saturating flashes.

a three-exponential component decay equation (44). The fast phase is attributable to the reoxidation of $Q_A^-$ by $Q_B$. The middle phase arises from $Q_A^-$ reoxidation in the PSII reaction center that has an empty $Q_B$ site at the time of the flash and has to bind to a plastoquinone (PQ) molecule from the PQ pool. The slow phase reflects $Q_A^-$ reoxida-

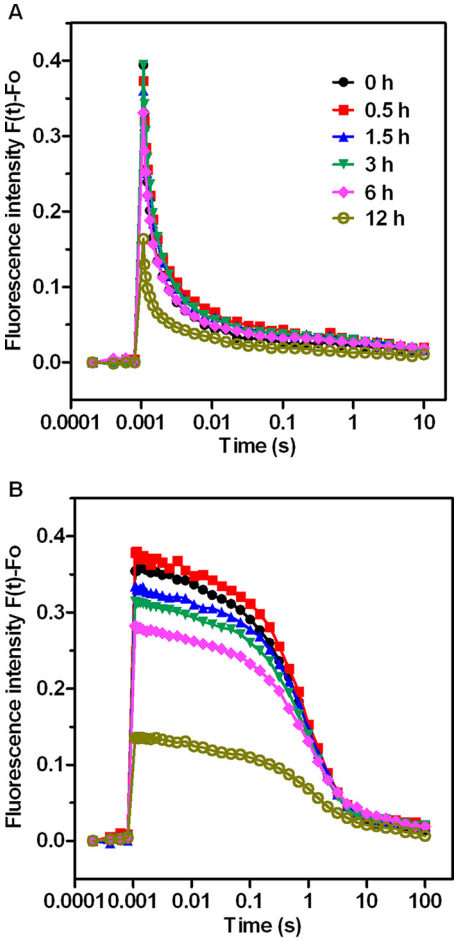


**FIG 7** $Q_A^-$ reoxidation kinetic curves of *Synechocystis* sp. treated with 70.4 mM (4×) $NO_2^-$ for various periods of time. (A) Fluorescence decay in the absence of DCMU. (B) Fluorescence decay in the presence of 20 $\mu$M DCMU. Each value represents the mean of the results from five replicates.

**TABLE 1** Decay kinetics of flash-induced variable fluorescence in *Synechocystis*[a]

| Time (h) | Fast-phase T1 ($\mu$s)/ A1 (%) | Middle-phase T2 (ms)/A2 (%) | Slow-phase T3 (s)/ A3 (%) | A0 (%) |
|---|---|---|---|---|
| Without DCMU | | | | |
| 0 | 128 ± 29/36.3 ± 2.8 | 1.3 ± 0.5/38.8 ± 0.3 | 0.06 ± 0.04/17.7 ± 5.8 | 7.2 ± 2.7 |
| 0.5 | 206 ± 11/38.0 ± 1.3 | 3.2 ± 0.1/37.6 ± 0.5 | 0.60 ± 0.11/16.1 ± 0.5 | 8.4 ± 0.3 |
| 1.5 | 242 ± 5/39.4 ± 2.6 | 3.3 ± 0.1/37.8 ± 0.4 | 1.82 ± 0.33/15.7 ± 2.3 | 7.1 ± 0.9 |
| 3 | 226 ± 4/39.1 ± 1.9 | 2.8 ± 0.2/38.8 ± 0.4 | 1.71 ± 0.48/15.8 ± 1.8 | 6.3 ± 0.7 |
| 6 | 198 ± 14/39.2 ± 0.2 | 2.6 ± 0.1/38.2 ± 0.4 | 0.99 ± 0.33/14.7 ± 0.6 | 7.9 ± 0.4 |
| 12 | 136 ± 9/37.8 ± 0.3 | 3.9 ± 0.3/37.3 ± 0.2 | 0.50 ± 0.30/15.8 ± 0.8 | 9.5 ± 1.0 |
| With DCMU | | | | |
| 0 | | | 0.96 ± 0.02/92.0 ± 1.2 | 8.0 ± 1.2 |
| 0.5 | | | 0.96 ± 0.00/91.7 ± 1.0 | 8.3 ± 0.6 |
| 1.5 | | | 1.06 ± 0.02/91.6 ± 1.1 | 8.4 ± 1.1 |
| 3 | | | 1.01 ± 0.03/91.1 ± 0.5 | 8.9 ± 0.5 |
| 6 | | | 1.05 ± 0.11/88.9 ± 1.9 | 11.1 ± 1.9 |
| 12 | | | 1.15 ± 0.24/86.9 ± 2.6 | 13.1 ± 2.6 |

[a]*Synechocystis* cells were treated with 70.4 mM (4×) $NO_2^-$ for the indicated periods of time, and relaxation of the flash-induced fluorescence yield with or without 20 $\mu$M DCMU was measured. The curves were analyzed in terms of three exponential components (fast, middle, and slow phases).

tion with the $S_2$ state of the oxygen-evolving complex, thus causing backward electron transport through the equilibrium of $Q_A^-Q_B$ and $Q_AQ_B^-$. The parameters of $Q_A^-$ reoxidation kinetics are summarized in Table 1. We found that $Q_A^-$ reoxidation kinetics rapidly respond to high levels of nitrite. Nitrite stress resulted in a significant increase in the decay half-life of the fast and middle phases. The time constant of the fast phase increased from 128 $\mu$s in control cells to 242 $\mu$s in cells subjected to a 3-h treatment with 4× $NO_2^-$. Furthermore, the time constant of the middle phase increased to 3.3 ms after 3 h of nitrite stress versus 1.3 ms in untreated control cells. However, high-nitrite treatment had no significant effects on the amplitudes of either the fast phase or the middle phase. These results suggest that salt stress retards $Q_B$-mediated $Q_A^-$ reoxidation and inhibits the binding of PQ molecules at the $Q_B$ binding site. On the other hand, the total fluorescence amplitudes were greatly decreased after 6 h of high-nitrite treatment, indicating a loss in $Q_A$ reduction, which correlates well with previous Chl fluorescence parameters (Fig. 3) and the original FI curve (Fig. S3).

When $Q_A^-$ reoxidation kinetics are determined in the presence of 20 $\mu$M DCMU, the fluorescence decay reflects $Q_A^-$ reoxidation via charge recombination with the $S_2$ state of the OEC (45). Analyses of these fluorescence relaxation curves showed that the fast and middle phases are converted to a slow phase with an approximately 2-s time constant (Table 1). In the first phase, there was no significant change in the time constant and its relative amplitude for this slow component. In contrast, the increase in the nondecaying component of fluorescence indicated that $Q_A^-$ is unable to recombine with the $S_2$ state, possibly because nitrite stress inactivates or reduces the Mn cluster during the second phase. In addition, the decrease in total fluorescence amplitudes in the presence of DCMU indicates that the reaction center is impaired. It has been suggested that total fluorescence amplitude in the DCMU-treated sample does not depend on the OEC as long as the reaction center is active, because a single electron provided by TyrZ or TyrD is sufficient to fully reduce $Q_A$ (46).

**Flash-induced fluorescence measurements of $PSII_X$ centers.** Measurements of the electron-transport capacity of the PSII reaction center reveal two distinct populations, active PSII ($PSII_A$) and inactive PSII ($PSII_X$) centers (47). In $PSII_A$ centers, the oxidation of $Q_A^-$ is fast (occurring in a few milliseconds or less), while in $PSII_X$ centers, the oxidation of $Q_A^-$ is much slower (48). We analyzed the fluorescence decay curves induced by a series of single-turnover flashes to determine the proportions of $PSII_X$ and $PSII_A$ in whole cells. The analysis is based on the fact that the fluorescence decay is controlled largely by the reoxidation kinetics of $Q_A^-$. Results of the S-state test of *Synechocystis* treated with excess nitrite for 12 h are shown in

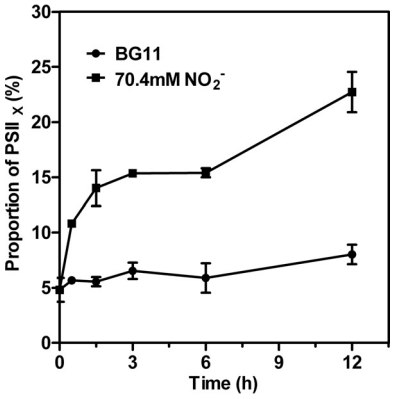


**FIG 8** The proportion of $PSII_X$ centers of *Synechocystis* treated with 70.4 mM (4×) $NO_2^-$ for various periods of time. Values are means ± SD ($n = 5$).

Fig. S4. The proportion of $PSII_X$ in whole cells was further estimated by conducting an S-state test (Fig. 8). The addition of nitrite resulted in a rapid increase in the percentage of $PSII_X$, from 4.8% at the beginning to 10.8% after 30 min. The population of $PSII_X$ centers increased linearly with prolonged exposure time, indicating that the proportion of $Q_B$ that cannot oxidize $Q_A^-$ increased.

**Effects of nitrite stress on PSII proteins.** To investigate if the decreased PSII activity in nitrite-stressed cells was associated with changes in the contents of PSII proteins, we further examined the effects of nitrite stress on several major PSII proteins. SDS-PAGE analysis of total cellular proteins isolated from untreated and salt-stressed cells did not reveal any pronounced changes in the polypeptide pattern (Fig. 9A). A more quantitative analysis of the PSII proteins was obtained by immunoblot analysis using antibodies (Fig. 9B). Compared with the results from untreated cells, the D1 and PsbO proteins were stable in the first phase of the response to excess nitrite. In contrast, the amounts of D1 protein during the second phase were decreased to about 16% and

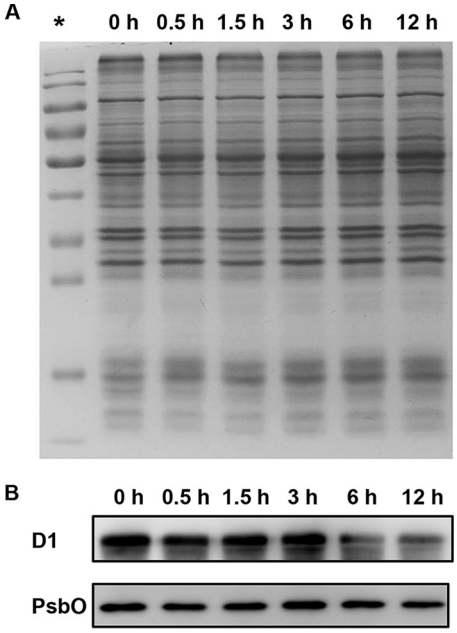


**FIG 9** Immunoblot analysis of PSII proteins. (A) SDS-PAGE of total proteins isolated from *Synechocystis* cells treated with 70.4 mM (4×) $NO_2^-$ for the indicated periods of time. Each sample corresponds to 10 $\mu$g protein. *, protein ladder. (B) Immunoblotting of the samples whose results are depicted in panel A was performed using antibodies specific for D1 and PsbO.

12% of the original value, respectively. PsbO was shown to degrade significantly only at the last time point, to a lesser extent than D1, with its amount declining to about 58% of that of total cellular proteins in untreated cells. Thus, excess-nitrite treatment damages the reaction center even faster and to a greater extent than it does the donor side of PSII in the second phase of the response to excess nitrite.

## DISCUSSION

External nitrite, which is transported via the same transporter as nitrate, can be transported into cells and used as the sole nitrogen source to support optimal growth. However, high nitrite concentrations are harmful to algae and higher plants (13, 22). Inhibition of photosynthesis has been reported to be one of the main targets of the toxic effects of high levels of nitrite. Consistent with these studies, *Synechocystis* proved to be sensitive to nitrite treatment, and millimolar concentrations of $NO_2^-$ drastically decreased the photosynthetic activity after short periods of incubation (Fig. 1). For nitrite to be assimilated by eukaryotic cells, it must be transported to the chloroplast across two membranes, where nitrite reductase catalyzes its reduction to ammonium. Reducing power for nitrite reduction is mainly supplied by the photosynthetic electron transport chain, which generates the requisite reduced Fd. Therefore, nitrite reduction is functionally coupled with photosynthesis, supporting the notion that photosynthetic processes are the prime targets of $NO_2^-$ toxicity.

In our experiments, PSII-dependent ($H_2O$-BQ) electron transport was inhibited to a much greater extent than was whole-chain activity (Fig. 2), indicating that the primary site of inhibition is localized to PSII rather than PSI or the intersystem electron transport (ET) components. Previous studies demonstrated that nitrite treatment inhibits the electron transport through PSII and stimulates electron flow through PSI by causing redistribution of the absorbed light energy in favor of the PSI (26, 28). Therefore, we contend that the PSII electron transfer was damaged more seriously than the whole-chain electron transfer and that the difference was possibly due to redistribution of absorbed excitation energy between two photosystems. The decrease in maximum chlorophyll fluorescence further demonstrates that PSII activity is inhibited by excess nitrite (Fig. 3).

As *Synechocystis* cells are more directly exposed to $NO_2^-$ in the environment than are plants, it is not surprising that cyanobacteria can absorb a considerable amount of nitrite in a relatively short period of time. Given that PSII activity in *Synechocystis* cells is inhibited rapidly in response to nitrite stress, the effects of nitrite stress on PSII could be manifested fast enough to separate the initial and subsequent effects. On the basis of the observations described above, the response of PSII to high levels of nitrite in *Synechocystis* cells can be divided into two phases. In the first phase, the relative variable fluorescence at the J step in nitrite-treated cells rises rapidly, reflecting the accumulation of $Q_A^-$ (Fig. 4A). This is in accordance with the observed changes in the JIP-test parameters. Nitrite stress resulted in a decrease in the efficiency of electron transfer from $Q_A^-$ to $Q_B$ ($\psi_0$), along with an increase in the initial slope of the relative variable fluorescence ($M_0$) (Fig. 4B). In addition, the proportion of $PSII_X$ centers, in which $Q_B$ cannot oxidize $Q_A^-$, increases in response to excess-nitrite treatment, as demonstrated by the S-state test (Fig. 8). Further, the $Q_A^-$ reoxidation kinetics showed that high levels of nitrite increased the half-life of the fast-phase and middle-phase components, indicating that the electron transport after $Q_A$ was hindered (Fig. 7 and Table 1). These results provide circumstantial evidence that the initial possible target of nitrite stress is the acceptor side of PSII and that inhibition of the acceptor side results in the inhibition of electron transfer from $Q_A^-$ to $Q_B$.

The retarded electron transfer between $Q_A^-$ and $Q_B$ may be due to the presence of a binding site for $NO_2^-$ near the plastoquinones on the stromal side of PSII. On the electron acceptor side of PSII, $Q_A$ (a one-electron acceptor plastoquinone) takes up one electron from $Phe_{D1}^-$ and transfers it to $Q_B$ (a two-electron acceptor plastoquinone). On the stromal side, the $Q_A$ binding pocket is formed by D2 and, analogously, the $Q_B$ pocket by D1. A bicarbonate ion ($HCO_3^-$) is bound to a nonheme iron (II) located

between $Q_A$ and $Q_B$ (36). The rate of electron transfer between plastoquinones depends on the coordinative properties of the nonheme iron (II) and the corresponding $HCO_3^-$ (49). It was previously reported that the inhibition induced by nitrite can be alleviated by the addition of bicarbonate (29). The accumulation of reduced $Q_A^-$ weakened the bond between bicarbonate and iron (50). Thus, we speculate that $NO_2^-$ competes with bicarbonate and binds to the nonheme iron (II), resulting in the inhibition of electron transfer from $Q_A^-$ to $Q_B$.

In the second phase of the response to $NO_2^-$ treatment, the $F_v/F_m$ ratio, which reflects the quantum efficiency of primary photochemical reactions, decreased markedly. The decrease in the $F_v/F_m$ ratio in nitrite-treated samples observed in this study suggests that the quantum efficiency of the reaction center is reduced. In parallel with $F_v/F_m$, nitrite stress resulted in a marked decrease in $F_m$ and an increase in $F_o$ (see Fig. S3 in the supplemental material). The increase in $F_o$ was accompanied by a significant increase in the proportion of the $Q_B$-non-reducing PSII centers (Fig. 8). Moreover, the level at the I step of the relative variable fluorescence curve was diminished after exposure to nitrite stress. Nitrite stress also resulted in decreases in the fluorescence levels at phases J, I, and P in the original FI curve. The O-J-I-P transient almost levelled off (Fig. S3). The effects described above are normally explainable by the impairment of the donor side or inactivation of the reaction center instead of inhibition of electron transport at the acceptor side of PSII.

To investigate the effects of nitrite stress on the donor side of PSII, we measured the changes of the TL glow curves in the absence and presence of DCMU. Both the B and Q TL bands depend on the $S_2$ states of the oxygen-evolving complex, and the parallel upshift of the peak temperatures of two bands in the second phase after the addition of nitrite (Fig. 5) reflects the increase in the redox stability of the $S_2$ state. The period-4 oscillation of the B band was more highly damped as a function of time after exposure to high-nitrite treatment than was the case with untreated control cells (Fig. 6). Our TL data are consistent with the observation of Sahay et al. (31) that nitrite inhibited the OEC on the donor side of PSII, as indicated by the suppression of the Q band and the upshift of the B band in nitrite-treated isolated chloroplasts. The increase in the stability of the $S_2$ state arises from the inactivation of the donor side (43). It has been reported that a mutant lacking the PsbO protein exhibits upshifts in the peak temperatures of $S_2Q_A^-$ and $S_2Q_B^-$ recombination, based on the TL profiles in a cyanobacterium, *Synechocystis* sp. strain PCC 6803 (42). In addition, removing PsbO from PSII preparations *in vitro* leads to an increase in the stability of the $S_2$ state, as revealed by the TL profiles and by the deactivation kinetics of the S states (51). Taking the data together, we propose that the increased stability of the $S_2$ state in the nitrite-stressed cells is due to the decreased amount of PsbO protein in these cells. To explore this possibility, we investigated the time course changes of the PsbO protein content. We found that nitrite stress indeed resulted in significant degradation of PsbO protein after 12 h. Immunoblot analysis (Fig. 7) also shows that the amount of D1 protein decreases together with PSII fluorescence and TL, further supporting our assumption that the decrease in PSII activity is accompanied by inactivation of the reaction center. Based on comparisons of the rates and extents of degradation between D1 and PsbO protein, we conclude that nitrite stress damages the reaction center even more rapidly and to a greater extent than the donor side of PSII in the second phase.

In light of our results and the published data, we propose that high levels of nitrite affect the photosynthesis of *Synechocystis* cells in two distinct phases. The first phase occurs within the first 3 h of exposure to excess nitrite. In this phase, the acceptor side of PSII is damaged, which greatly retards electron transfer between $Q_A^-$ and $Q_B$. In the second phase, which proceeds from 6 to 12 h after nitrite treatment, nitrite inactivates the reaction center and inhibits electron transfer at the donor side, which are results associated with the degradation of D1 and PsbO proteins in PSII. Furthermore, the reaction center is a more sensitive target of nitrite stress than is the donor side of PSII. Our results therefore broaden the incomplete view that the donor side of PSII is the primary target of nitrite stress (31).

## MATERIALS AND METHODS

**Growth conditions and nitrite treatment.** *Synechocystis* sp. strain PCC 6803, provided by the Culture Collection of Pasteur Institute in Paris, France, was grown photoautotrophically in BG11 medium containing 17.6 mmol liter$^{-1}$ $NaNO_3$ (52). Cultures were aerated with filtered air at 30°C and illuminated continuously with white fluorescent light consisting of 40 $\mu$mol photons m$^{-2}$ s$^{-1}$. BG11 lacking $NaNO_3$ was used as N-deficient medium (N-medium). For nitrite treatment, cells in the exponential-growth phase (optical density at 730 nm [$OD_{730}$], 0.8 to 1.0) were harvested, washed twice with N-medium, and resuspended in modified BG11 medium (using $NaNO_2$ instead of $NaNO_3$ as the N source). Nitrite solution was filtered through a 0.22-mm-pore-size filter membrane before use and then added to the modified BG11 medium to achieve final nitrite concentrations of 17.6, 35.2, 52.8, and 70.4 mM (1×, 2×, 3×, and 4× $NO_2^-$, respectively). The initial cell density was set to an $OD_{730}$ of 0.1. The algal pellet was incubated in BG11 media under the same conditions as were used for the control. The growth of cell cultures was assessed by monitoring the optical density at 730 nm with a UV-1800PC spectrophotometer (Shanghai, China).

**Chl fluorescence analysis.** Chl fluorescence was detected using an AquaPen-C AP-C 100 instrument (Photon Systems Instruments, Brno, Czech Republic). After the cells were fully dark adapted for 15 min, the minimal fluorescence level ($F_o$) was measured under conditions of illumination with weak blue light (<1 $\mu$mol m$^{-2}$ s$^{-1}$) at 450 nm that was sufficiently low in intensity to avoid inducing any significant variable fluorescence. An 800-ms flash of saturating white light (8,000 $\mu$mol m$^{-2}$ s$^{-1}$) was then given to determine the maximal fluorescence level ($F_m$) with or without 20 $\mu$M 3-(3,4-dichlorophenyl)-1,1-dimethylurea (DCMU) as described by Ogawa and Sonoike (53). The maximum quantum yields of PSII photochemistry were calculated as $F_v/F_m = (F_m - F_o)/F_m$ in accordance with the method described by Genty et al. (54).

**Estimation of electron transport activities.** The whole-chain or PSII-mediated electron transport rates in intact cells were estimated by measuring $O_2$ evolution using a Clark-type electrode (Oxylab 2; Hansatech, UK) at 30°C as described by Wang et al. (55). Cell cultures were adjusted to an $OD_{730}$ of 2.0 with fresh BG11 for all of the measurements. The whole-chain electron transport ($H_2O$ to $CO_2$) rate was measured using water as the electron donor in the presence of 10 mM $NaHCO_3$. The PSII-mediated reaction mixture (5 mM $NH_4Cl$, 4 mM $K_3FeCN$, and 1 mM phenyl-p-benzoquinone [BQ]) was used to measure the rate of electron transport from $H_2O$ to $Q_B$ through PSII. $O_2$ evolution was followed at a saturating light level of 500 $\mu$mol photons m$^{-2}$ s$^{-1}$ for 5 min, and the rate was calculated accordingly (56).

**Polyphasic Chl *a* fluorescence induction and the JIP test.** Polyphasic Chl *a* fluorescence induction (FI) was carried out at room temperature using an FL-3500 dual-modulation kinetic fluorometer (Photon Systems Instruments, Brno, Czech Republic), as described elsewhere (34, 35). Briefly, 3-ml samples of microalgal cells ($OD_{730}$ of 1.0) were dark adapted for 20 min prior to measurement. Since the maximum detected fluorescence value for the FL-3500 fluorometer is 3.0000 V, a 20% detector gain setting was used for all measurements to ensure that the highest value (P step) did not exceed two-thirds of the limit. Under conditions of continuous red actinic light (625 nm) at high intensity, the FI was recorded for a period of 1 s on a logarithmic time scale, with data acquisition every of 10 $\mu$s for the first 2 ms and for every ms thereafter. The FI kinetics are given as the fluorescence value $F_t$ at any time *t*. The fluorescence rise follows a regular pattern of O-J-I-P, with two intermediate steps, J (at 2 ms) and I (at 20 ms), between the initial O ($F_o$) and the maximum P ($F_p$) fluorescence. Different samples may exhibit fluorescence signals of different amplitudes. To convert these signals into a form that can be used for comparisons, the relative variable fluorescence V at any time *t* is obtained by a mathematical equation defined as $V_t = (F_t - F_o)/(F_m - F_o)$. The variable part of any fluorescence induction kinetics can thus be presented on a scale from zero to unity ($0 \leq V_t \leq 1$).

The JIP test was developed for quantitative analysis of the O-J-I-P transient according to Strasser et al. (57). In the present study, the following JIP test parameters were calculated to quantify PSII behavior as follows: $V_J$ [$V_J = (F_J - F_o)/(F_m - F_o)$], relative variable fluorescence at level J; $M_0$ or $(dV/dt)_0$ [$M_0 = 4 (F_{300\ \mu s} - F_o)/(F_m - F_o)$], the initial slope, indicating the net closing rate of the reaction center; $\psi_0$ ($\psi_0 = ET_0/TR_0 = 1 - V_J$), the probability that a trapped exciton moves an electron into the electron transport chain beyond $Q_A$ (at $t = 0$). For the last equation, the energy flux corresponding to the electron transport beyond $Q_A^-$ is indicated as ET; the excitation energy flux which reaches the reaction center and gets trapped there (in the sense of leading to $Q_A$ reduction) is indicated as trapping flux TR.

**Measurement of $Q_A^-$ reoxidation kinetics.** The $Q_A^-$ reoxidation kinetics after a single-turnover flash were monitored with an FL-3500 dual-modulation kinetic fluorometer (Photon Systems Instruments, Brno, Czech Republic), as described by Nedbal et al. (58). All samples were concentrated to an $OD_{730}$ of 1.0 and dark adapted for 20 min prior to measurement. The experimental protocol in this instrument measures $F_o$, executes a single-turnover flash to reduce the $Q_A$ acceptor, and follows the subsequent decline of fluorescence that reflects the reoxidation kinetics. Both the measuring flash (4 $\mu$s) and actinic flashes (50 $\mu$s) were provided by computer-controlled light-emitting diodes.

According to Beauchemin et al. (44), the $Q_A^-$ reoxidation kinetics curves are fitted by the following three-component exponential equation:

$$F(t) = A_1 \exp\ (-t/T_1) + A_2 \exp\ (-t/T_2) + A_3 \exp\ (-t/T_3) + A_0$$

where F(*t*) is the variable fluorescence yield, $A_0$ to $A_3$ are the amplitudes, and $T_1$ to $T_3$ are the time constants from which the half-life values can be calculated as $t_{1/2} = \ln 2T$.

**S-state test.** To further determine the proportion of inactive PSII centers ($PSII_X$), S-state tests were performed (47, 48). The $F_o$ fluorescence was measured during the first 1-ms exposure to measuring light. Ten actinic flashes were then fired in 100-ms intervals to advance the S states. After each actinic flash, the fluorescence decay was measured on a logarithmic time scale with 8 data points per decade. The population of $PSII_X$ centers was estimated by the difference between $F_o$ and the fluorescence level

measured at 100 ms after the fourth flash ($\Delta F_4 = F_{400\ ms}/F_o - 1$), which is controlled almost entirely by inactive centers. Given the decreased relative variable fluorescence, a revised equation was proposed according to Pan et al. (59), as follows: $PSII_X$ (%) $= \Delta F_4 \times 100/(F_{300\ ms}/F_o - 1)$.

**Thermoluminescence measurements.** Thermoluminescence (TL) measurements of whole cells were performed with a TL 400/PMT thermoluminescence system (Photon Systems Instruments, Brno, Czech Republic). The cultures were concentrated to an $OD_{730}$ of 5.0, and 50 $\mu$l of the samples was taken for each measurement. After 20 min of dark adaptation at 30°C, the cells were cooled to 0°C and illuminated with one single-turnover flash. The cells were then warmed to 60°C at a heating rate of 1°C · $s^{-1}$, and the TL light emission was measured during the heating. The Q TL band was detected in the presence of 20 $\mu$M DCMU to block the electron flow beyond $Q_A$ before the flash illumination. To detect period-4 oscillation of the B band, cells were illuminated with a short series of single-turnover flashes (ranging from 1 to 6 flashes).

**SDS-PAGE analysis and immunoblotting.** Total cellular proteins were extracted from *Synechocystis* cells as described by Chen et al. (60) with minor modifications. Cells were harvested and resuspended in lysis buffer (40 mM Tris-HCl [pH 8.0]) supplemented with 1 mM phenylmethanesulfonyl fluoride (PMSF) as the protease inhibitor. The cells were lysed using sonication (3 s on, 3 s off) for 20 min on ice with a JY92-IIN sonicator (Ningbo Scientz Biotechnology Co., Ltd.), which had an output of 135 W. The whole-cell lysate was centrifuged (Eppendorf 5810R centrifuge) at 1,800 × g for 10 min at 4°C to remove cell debris. Protein concentrations were estimated with the Bradford assay.

Equal amounts (10 $\mu$g) of proteins were separated by 12% SDS–PAGE, stained with Coomassie brilliant blue R250, or transferred to polyvinylidene fluoride (PVDF) membranes (GE Healthcare). After blocking for 1 h with 5% milk was performed, membranes were probed using rabbit primary anti-D1 and anti-PsbO antibodies (1:5,000), followed by secondary antibody conjugated to horseradish peroxidase (1:5,000). The labeled proteins were detected by chemiluminescence using SuperSignal West Pico chemiluminescent substrate (Thermo Fisher Scientific), and the signals were visualized using an ImageQuant LAS 4000 Mini system (GE Healthcare).

**Statistical analyses.** The experiments were performed in biological triplicate, and the results are presented as means or means ± standard deviations (SD). Data analysis was performed using SPSS-13, and significance was determined at a confidence limit of 95% or 99%. The significant differences between the control and test values were tested using one-way ANOVA, and differences were considered to be significant at a $P$ value of $<0.05$ or a $P$ value of $<0.01$.

## SUPPLEMENTAL MATERIAL

Supplemental material for this article may be found at https://doi.org/10.1128/AEM.02952-16.

**TEXT S1**, PDF file, 0.4 MB.

## ACKNOWLEDGMENTS

We are thankful to EcoTech (Beijing) for FL3500 support.

This work was supported jointly by the National Program on Key Basic Research Project (2012CB224803), the National Natural Science Foundation of China (31270094 and 31300030), and the State Key Laboratory of Freshwater Ecology and Biotechnology (2016FB11). The funders had no role in study design, data collection and interpretation, or the decision to submit the work for publication.

## REFERENCES

1. Galloway JN, Townsend AR, Erisman JW, Bekunda M, Cai Z, Freney JR, Martinelli LA, Seitzinger SP, Sutton MA. 2008. Transformation of the nitrogen cycle: recent trends, questions, and potential solutions. Science 320:889–892. https://doi.org/10.1126/science.1136674.
2. Camargo JA, Alonso A. 2006. Ecological and toxicological effects of inorganic nitrogen pollution in aquatic ecosystems: a global assessment. Environ Int 32:831–849. https://doi.org/10.1016/j.envint.2006.05.002.
3. Philips S, Laanbroek HJ, Verstraete W. 2002. Origin, causes and effects of increased nitrite concentrations in aquatic environments. Rev Environ Sci Biotechnol 1:115–141. https://doi.org/10.1023/A:1020892826575.
4. Braida W, Ong SK. 2000. Decomposition of nitrite under various pH and aeration conditions. Water Air Soil Pollut 118:13–26. https://doi.org/10.1023/A:1005193313166.
5. Razumov V, Tyutyunova F. 2001. Nitrite contamination of the Moskva River: causes and effects. Water Resour 28:324–334. https://doi.org/10.1023/A:1010409009477.
6. Okafor PN, Ogbonna UI. 2003. Nitrate and nitrite contamination of water sources and fruit juices marketed in south-eastern Nigeria. J Food Compos Anal 16:213–218. https://doi.org/10.1016/S0889-1575(02)00167-9.
7. Rawat SK, Singh RK, Singh RP. 2012. Remediation of nitrite contamination in ground and surface waters using aquatic macrophytes. J Environ Biol 33:51–56.
8. Laryushkin-Zheleznyi B, Novikov A. 2005. On the distribution of mineral nitrogen forms in polluted river reaches in urban territories. Water Resour 32:537–544. https://doi.org/10.1007/s11268-005-0068-2.
9. Li Y, Wan W, Song J, Wu Y, Xu Y, Zhang M. 2009. Classification of groundwater contamination in Yuxi River Valley, Shaanxi Province, China. Bull Environ Contam Toxicol 82:234–238. https://doi.org/10.1007/s00128-008-9608-1.
10. Schuch R, Gensicke R, Merkel K, Winter J. 2000. Nitrogen and DOC removal from wastewater streams of the metal-working industry. Water Res 34:295–303. https://doi.org/10.1016/S0043-1354(99)00109-8.
11. Chen W, Zhang S, Rong J, Li X, Chen H, He C, Wang Q. 2016. Effective biological DeNOx of industrial flue gas by the mixotrophic cultivation of an oil-producing green alga Chlorella sp. C2. Environ Sci Technol 50:1620–1627. https://doi.org/10.1021/acs.est.5b04696.
12. Zhang X, Chen H, Chen W, Qiao Y, He C, Wang Q. 2014. Evaluation of an oil-producing green alga Chlorella sp. C2 for biological DeNOx of industrial flue gases. Environ Sci Technol 48:10497–10504. https://doi.org/10.1021/es5013824.
13. Yang SL, Wang J, Cong W, Cai ZL, Fan OY. 2004. Utilization of nitrite as

a nitrogen source by Botryococcus braunii. Biotechnol Lett 26:239–243. https://doi.org/10.1023/B:BILE.0000013722.45527.18.
14. Reference deleted.
15. Córdoba F, Cárdenas J, Fernández E. 1986. Kinetic characterization of nitrite uptake and reduction by Chlamydomonas reinhardtii. Plant Physiol 82:904–908. https://doi.org/10.1104/pp.82.4.904.
16. Luque I, Flores E, Herrero A. 1993. Nitrite reductase gene from Synechococcus sp. PCC-7942: homology between cyanobacterial and higher-plant nitrite reductases. Plant Mol Biol 21:1201–1205. https://doi.org/10.1007/BF00023618.
17. Flores E, Frias JE, Rubio LM, Herrero A. 2005. Photosynthetic nitrate assimilation in cyanobacteria. Photosynth Res 83:117–133. https://doi.org/10.1007/s11120-004-5830-9.
18. Tischner R. 2000. Nitrate uptake and reduction in higher and lower plants. Plant Cell Environ 23:1005–1024. https://doi.org/10.1046/j.1365-3040.2000.00595.x.
19. Nagore D, Sanz B, Soria J, Llarena M, Llama MJ, Calvete JJ, Serra JL. 2006. The nitrate/nitrite ABC transporter of Phormidium laminosum: phosphorylation state of NrtA is not involved in its substrate binding activity. Biochim Biophys Acta 1760:172–181. https://doi.org/10.1016/j.bbagen.2005.12.011.
20. Aichi M, Takatani N, Omata T. 2001. Role of NtcB in activation of nitrate assimilation genes in the cyanobacterium Synechocystis sp. strain PCC. 6803. J Bacteriol 183:5840–5847. https://doi.org/10.1128/JB.183.20.5840-5847.2001.
21. Ohashi Y, Shi W, Takatani N, Aichi M, Maeda S, Watanabe S, Yoshikawa H, Omata T. 2011. Regulation of nitrate assimilation in cyanobacteria. J Exp Bot 62:1411–1424. https://doi.org/10.1093/jxb/erq427.
22. Abe K, Imamaki A, Hirano M. 2002. Removal of nitrate, nitrite, ammonium and phosphate ions from water by the aerial microalga Trentepohlia aurea. J Appl Phycol 14:129–134. https://doi.org/10.1023/A:1019599216554.
23. Chen WM, Liu H, Zhang QM, Dai SG. 2011. Effect of nitrite on growth and microcystins production of Microcystis aeruginosa PCC7806. J Appl Phycol 23:665–671. https://doi.org/10.1007/s10811-010-9558-y.
24. Chen WM, Liu H. 2015. Intracellular nitrite accumulation: the cause of growth inhibition of Microcystis aeruginosa exposure to high nitrite level. Phycol Res 63:197–201. https://doi.org/10.1111/pre.12090.
25. Serrano A, Rivas J, Losada M. 1981. Nitrate and nitrite as 'in vivo' quenchers of chlorophyll fluorescence in blue-green algae. Photosynth Res 2:175–184. https://doi.org/10.1007/BF00032356.
26. Singh P, Jajoo A, Sahay A, Bharti S. 2007. Relation between the mode of binding of nitrite and the energy distribution between the two photosystems. Physiol Plant 129:447–454.
27. Loranger C, Carpentier R. 1994. A fast bioassay for phytotoxicity measurements using immobilized photosynthetic membranes. Biotechnol Bioeng 44:178–183. https://doi.org/10.1002/bit.260440206.
28. Sahay A, Jajoo A, Singh P, Bharti S. 2006. Nitrite regulates distribution of excitation energy between the two photosystems by causing state transition. Plant Physiol Biochem 44:7–12. https://doi.org/10.1016/j.plaphy.2006.01.004.
29. Stemler A, Murphy JB. 1985. Bicarbonate-reversible and irreversible inhibition of photosystem II by monovalent anions. Plant Physiol 77:974–977. https://doi.org/10.1104/pp.77.4.974.
30. Sinclair J. 1987. Changes in spinach thylakoid activity due to nitrite ions. Photosynth Res 12:255–263. https://doi.org/10.1007/BF00055125.
31. Sahay A, Jajoo A, Bharti S. 2006. A thermoluminescence study of the effects of nitrite on photosystem II in spinach thylakoids. Luminescence 21:143–147. https://doi.org/10.1002/bio.898.
32. Jajoo A, Bharti S, Kawamori A. 2005. EPR characteristics of chloride-depleted photosystem II membranes in the presence of other anions. Photochem Photobiol Sci 4:459–462. https://doi.org/10.1039/b414849e.
33. Inoue N, Emi T, Yamane Y, Kashino Y, Koike H, Satoh K. 2000. Effects of high-temperature treatments on a thermophilic cyanobacterium Synechococcus vulcanus. Plant Cell Physiol 41:515–522. https://doi.org/10.1093/pcp/41.4.515.
34. Strasser RJ, Srivastava A, Govindjee. 1995. Polyphasic chlorophyll a fluorescence transient in plants and cyanobacteria. Photochem Photobiol 61:32–42. https://doi.org/10.1111/j.1751-1097.1995.tb09240.x.
35. Pospísil P, Dau H. 2000. Chlorophyll fluorescence transients of photosystem II membrane particles as a tool for studying photosynthetic oxygen evolution. Photosynth Res 65:41–52. https://doi.org/10.1023/A:1006469809812.
36. Stirbet A, Govindjee. 2012. Chlorophyll a fluorescence induction: a personal perspective of the thermal phase, the J-I-P rise. Photosynth Res 113:15–61. https://doi.org/10.1007/s11120-012-9754-5.
37. Zhu XG, Govindjee, Baker NR, deSturler E, Ort DR, Long SP. 2005. Chlorophyll a fluorescence induction kinetics in leaves predicted from a model describing each discrete step of excitation energy and electron transfer associated with photosystem II. Planta 223:114–133. https://doi.org/10.1007/s00425-005-0064-4.
38. Lu C, Vonshak A. 2002. Effects of salinity stress on photosystem II function in cyanobacterial Spirulina platensis cells. Physiol Plant 114:405–413. https://doi.org/10.1034/j.1399-3054.2002.1140310.x.
39. Strasser BJ. 1997. Donor side capacity of photosystem II probed by chlorophyll a fluorescence transients. Photosynth Res 52:147–155. https://doi.org/10.1023/A:1005896029778.
40. Ducruet JM, Vass I. 2009. Thermoluminescence: experimental. Photosynth Res 101:195–204. https://doi.org/10.1007/s11120-009-9436-0.
41. Sane PV, Ivanov AG, Öquist G, Hüner NPA. 2012. Thermoluminescence, p 445–474. *In* Eaton-Rye JJ, Tripathy BC, Sharkey TD (ed), Photosynthesis: plastid biology, energy conversion and carbon assimilation, advances in photosynthesis and respiration, vol 34. Springer, Dordrecht, Netherlands.
42. Burnap RL, Shen J, Jursinic PA, Inoue Y, Sherman LA. 1992. Oxygen yield and thermoluminescence characteristics of a cyanobacterium lacking the manganese-stabilizing protein of photosystem II. Biochemistry 31:7404–7410. https://doi.org/10.1021/bi00147a027.
43. Gong H, Tang Y, Wang J, Wen X, Zhang L, Lu C. 2008. Characterization of photosystem II in salt-stressed cyanobacterial Spirulina platensis cells. Biochim Biophys Acta 1777:488–495. https://doi.org/10.1016/j.bbabio.2008.03.018.
44. Beauchemin R, Gauthier A, Harnois J, Boisvert S, Govindachary S, Carpentier R. 2007. Spermine and spermidine inhibition of photosystem II: disassembly of the oxygen evolving complex and consequent perturbation in electron donation from TyrZ to P680+ and the quinone acceptors QA- to QB. Biochim Biophys Acta 1767:905–912. https://doi.org/10.1016/j.bbabio.2007.04.001.
45. Vass I, Kirilovsky D, Etienne AL. 1999. UV-B radiation-induced donor- and acceptor-side modifications of photosystem II in the cyanobacterium Synechocystis sp. PCC 6803. Biochemistry 38:12786–12794.
46. Tóth T, Zsiros O, Kis M, Garab G, Kovács L. 2012. Cadmium exerts its toxic effects on photosynthesis via a cascade mechanism in the cyanobacterium, Synechocystis PCC 6803. Plant Cell Environ 35:2075–2086. https://doi.org/10.1111/j.1365-3040.2012.02537.x.
47. Lavergne J, Leci E. 1993. Properties of inactive Photosystem II centers. Photosynth Res 35:323–343. https://doi.org/10.1007/BF00016563.
48. Kaftan D, Meszaros T, Whitmarsh J, Nedbal L. 1999. Characterization of photosystem II activity and heterogeneity during the cell cycle of the green alga Scenedesmus quadricauda. Plant Physiol 120:433–442. https://doi.org/10.1104/pp.120.2.433.
49. Wodala B, Deak Z, Vass I, Erdei L, Altorjay I, Horvath F. 2008. In vivo target sites of nitric oxide in photosynthetic electron transport as studied by chlorophyll fluorescence in pea leaves. Plant Physiol 146:1920–1927. https://doi.org/10.1104/pp.107.110205.
50. Goussias C, Deligiannakis Y, Sanakis Y, Ioannidis N, Petrouleas V. 2002. Probing subtle coordination changes in the iron-quinone complex of photosystem II during charge separation, by the use of NO. Biochemistry 41:15212–15223. https://doi.org/10.1021/bi026223e.
51. Kuwabara T, Murata N. 1983. Quantitative analysis of the inactivation of photosynthetic oxygen evolution and the release of polypeptides and manganese in the photosystem II particles of spinach chloroplasts. Plant Cell Physiol 24:741–747.
52. Stanier RY, Kunisawa R, Mandel M, Cohen-Bazire G. 1971. Purification and properties of unicellular blue-green algae (order Chroococcales). Bacteriol Rev 35:171–205.
53. Ogawa T, Sonoike K. 2016. Effects of bleaching by nitrogen deficiency on the quantum yield of photosystem II in Synechocystis sp. PCC 6803 revealed by Chl fluorescence measurements. Plant Cell Physiol 57:558–567.
54. Genty B, Briantais J-M, Baker NR. 1989. The relationship between the quantum yield of photosynthetic electron transport and quenching of chlorophyll fluorescence. Biochim Biophys Acta 990:87–92. https://doi.org/10.1016/S0304-4165(89)80016-9.
55. Wang Q, Jantaro S, Lu B, Majeed W, Bailey M, He Q. 2008. The high light-inducible polypeptides stabilize trimeric photosystem I complex under high light conditions in Synechocystis PCC 6803. Plant Physiol 147:1239–1250. https://doi.org/10.1104/pp.108.121087.
56. Li W, Gao H, Yin C, Xu X. 2012. Identification of a novel thylakoid protein gene involved in cold acclimation in cyanobacteria. Microbiology 158:2440–2449. https://doi.org/10.1099/mic.0.060038-0.

57. Strasser RJ, Srivastava A, Tsimilli-Michael M. 2000. The fluorescence transient as a tool to characterize and screen photosynthetic samples, p 445–483. *In* Yunus M, Pathre U, Mohanty P (ed), Probing photosynthesis: mechanisms, regulation and adaptation. CRC Press, Boca Raton, FL.
58. Nedbal L, Trtilek M, Kaftan D. 1999. Flash fluorescence induction: a novel method to study regulation of photosystem II. J Photochem Photobiol B Biol 48:154–157. https://doi.org/10.1016/S1011-1344(99)00032-9.
59. Pan X, Deng C, Zhang D, Wang J, Mu G, Chen Y. 2008. Toxic effects of amoxicillin on the photosystem II of Synechocystis sp. characterized by a variety of in vivo chlorophyll fluorescence tests. Aquat Toxicol 89: 207–213. https://doi.org/10.1016/j.aquatox.2008.06.018.
60. Chen Z, Zhan J, Chen Y, Yang M, He C, Ge F, Wang Q. 2015. Effects of phosphorylation of beta subunits of phycocyanins on state transition in the model cyanobacterium Synechocystis sp. PCC 6803. Plant Cell Physiol 56: 1997–2013.